Published in final edited form as:
Nanomedicine (Lond). 2011 July ; 6(5): 777–791. doi:10.2217/nnm.11.73.

Cellular uptake mechanisms and toxicity of quantum dots in dendritic cells

Leshuai W Zhang[1], **Wolfgang Bäumer**[2], and **Nancy A Monteiro-Riviere**[1,†]

[1]Center for Chemical Toxicology Research & Carolina State University, Raleigh, NC 27606, USA

[2]Institute of Pharmacology, Toxicology & Pharmacy, University of Veterinary Medicine Hannover, Foundation, Hannover, Germany

Abstract

Quantum dots (QDs) are nanoparticles with strong fluorescent emission and are novel tools used in biomedical applications, but the toxicity and mechanism of cellular uptake are poorly understood. QD655-COOH (negative charge, 18 nm) consist of a cadmium/selenide core and a zinc sulfide shell with a carboxylic acid coating with an emission wavelength of 655 nm.

Materials & Methods—Peripheral blood mononuclear cells were isolated from porcine blood by gradient centrifugation, and monocytes, which are CD14 positive, were purified. Monocytes were differentiated into dendritic cells (DCs) with GM-CSF and IL-4.

Results—Monocytes showed cellular uptake of QD655-COOH, while lymphocytes did not. Monocyte differentiation into DCs increased the cellular uptake by sixfold when dosed with 2 nM of QD655-COOH. Transmission electron microscopy depicted QD655-COOH in the cytoplasmic vacuoles of DCs. Twelve endocytic inhibitors demonstrated QD655-COOH endocytosis in DCs, which was recognized by clathrin and scavenger receptors and regulated by F-actin and phospholipase C. In addition, DC maturation with lipopolysaccharide (LPS) caused an increase in QD655-COOH uptake compared with DCs without LPS stimulation. Viability assays, including 96AQ, CCK-8, alamar blue and ApoTox, exhibited minimal toxicity in DCs dosed with QD655-COOH at 24 h. However, glutathione levels showed a significant decrease with 10 nM of QD655-COOH. Finally, QD655-COOH exposure was associated with a decrease in CD80/CD86 expression after LPS stimulation, suggesting suppression with DC maturation.

Conclusion—These findings shed light on the mechanism of QD655-COOH uptake in DCs and that cellular uptake pathways are dependent on cell type and cell differentiation.

[†]Author for correspondence: Tel.: +1 919 513 6426, Fax: +1 919 513 6358, nancy_monteiro@ncsu.edu.

Ethical conduct of research

The authors state that they have obtained appropriate institutional review board approval or have followed the principles outlined in the Declaration of Helsinki for all human or animal experimental investigations. In addition, for investigations involving human subjects, informed consent has been obtained from the participants involved.

Financial & competing interests disclosure

This work was supported by a grant from the NIH (RO1 ES016138) and the US Air Force Office of Scientific Research (AFOSR) Grant (FA 9550-08-1-0182). The authors have no other relevant affiliations or financial involvement with any organization or entity with a financial interest in or financial conflict with the subject matter or materials discussed in the manuscript apart from those disclosed.

No writing assistance was utilized in the production of this manuscript.

Keywords

cellular uptake; dendritic cells; endocytosis; LPS; nanoparticles; quantum dot nanoparticles; scavenger receptor

The rapid growth in the nanotechnology industry leads to novel nanomaterials for biomedical applications, such as diagnostics, drug delivery and nanotherapy, yet the knowledge regarding the cellular uptake mechanisms of nanoparticles (NPs) and toxicity to cells is not well understood. NPs with certain physicochemical characteristics can readily enter cells. Human epidermal keratinocytes (HEKs) have the capacity to take up unfunctionalized multiwall carbon nanotubes [1], carbon black [2], functionalized fullerenes [3,4] and functionalized single-walled carbon nanotubes [5], and these NPs have been localized in the cytoplasmic vacuoles of HEKs. In addition to carbon-based NPs, metal-based nanomaterials such as gold [6], silver [7] and aluminum [8] NPs can easily become incorporated into cells.

Quantum dots (QDs) are of special interest because they can be used as fluorescent probes for cellular imaging and diagnostics. In addition to their strong fluorescence intensity, their stability, water solubility, small size and flexible surface charge enable QD suitable agents to study intracellular tracking with *in vitro* and *in vivo* studies. QDs typically consist of a cadmium/selenide (CdSe) core with a zinc sulfide (ZnS) shell with some type of surface coating. Negatively and positively charged QDs can be incorporated into other human cell types [9,10]. Our laboratory has shown that QDs with a cadmium sulfide (CdS) shell [11] or ZnS shell [12–14] can enter HEKs. Specific mechanisms of QD cellular uptake in HEKs has been investigated [15]. However, QD cellular uptake regulation in other cell types, such as dendritic cells (DCs) is not well known.

Dendritic cells play an important role in initiating the immune response owing to their efficient cell uptake, presentation of antigen and the ability of cytokine production. DC express MHCII and CD80/CD86 on the cell surface and enhanced levels of these surface markers have been found in mature DCs. Human DCs are derived from bone marrow cells [16] in the presence of GM-CSF and the cytokine IL-4. Functional DCs can be derived from peripheral blood monocytes in human, mouse and bovine cells [17–19]. Monocytes move from the blood to the site of injury or infection and differentiate into macrophages or DCs followed by the release of proinflammatory mediators. Since DCs can effectively engulf NPs and present antigen released from nanovectors, vaccine development has been focused on DC cellular uptake [20–22]. Gelatin NPs can be phagocytozed by DCs generated from murine bone marrow cells localized in lysosomes [23]. Understanding the specific endocytic mechanism and the potential for immunocytotoxicity of DCs may provide new insights into vaccine delivery.

Nonfunctionalized QDs were localized in cells and the cellular uptake was size dependent in human blood monocyte-derived macrophages [24]. However, to date, there are no reports on the endocytic mechanism or toxicity of QDs in monocyte-derived DCs. In this study, we used porcine monocyte-derived DCs as an *in vitro* model. Genetically and physiologically, pigs are more similar to humans compared with rodents. Porcine blood is closer in similarity to human blood in that their antigen-presenting cells, such as monocytes, DC precursors and fibrocytes, are similar. Second, porcine plasmacytoid DCs can produce high quantities of IFN-α and TNF, similar to humans, but distinct from the mouse model [25]. Third, porcine dendritic cells derived from monocytes behave similarly to mouse or human DCs with the increased level of surface costimulatory molecules, such as CD80/CD86 and MHCI/II, providing signals to initiate T-cell activation, when DCs were matured [26,27]. Fourth, most

of the antibodies for human DCs markers can recognize porcine DCs, indicating the structural similarity of DC surface markers between two species [28]. Finally, the porcine model can provide a large amount of blood with sufficient supply of monocytes for one study compared with the murine model, which requires more than five mice to get a sufficient quantity of blood. Therefore, porcine monocyte-derived DCs may serve as a good *in vitro* model for nanoimmunotoxicology. The objective of this study is to determine the cytotoxicity, localization of QD655-COOH cellular uptake in lymphocytes, monocytes and monocyte-derived DCs and QD655-COOH endocytic mechanisms, and to compare them with previous studies of QD cellular uptake in HEKs. In addition, we investigated the optimal viability assay for DCs and the effect of DC maturation and toxicity with QD655-COOH.

Materials & methods

Quantum dots

Quantum dots (Invitrogen, Carlsbad, CA, USA) with emission maxima at 655 nm are ellipsoid shaped, with a CdSe core/zinc sulfide shell with a 6 nm (minor axis) ×12 nm (major axis) diameter. QD655 coated with polyethylene glycol (PEG;neutral), PEG-amine (NH_2, positive charged) or carboxylic acid (COOH, negative charged) have hydrodynamic sizes of 45 nm (PEG), 18 nm (COOH) and 20 nm (NH_2), respectively. QDs were supplied at concentrations ranging from 2 to 8.7 mM in a 50 mM borate buffer of pH 9.0 (carboxylic acid-coated QDs) or pH 8.3 (PEG and PEG-amine-coated QDs). The size distribution is estimated at 3% based on transmission electron microscopy (TEM). Typically, it is estimated that there are 800–1200 carboxylic acid molecules per QD (Molecular Probe/InVitrogen). The polydispersity index measurement is not particularly useful for an engineered construct such as this due to the large dissimilarity between the molecular weights of the constituents (e.g., cadmium vs carbon) and is not provided by the manufacturer. Additional details on the physicochemical properties of these QDs can be found in our previous publications [12,15].

Generation of DCs from peripheral blood monocytes

Pig peripheral blood mononuclear cells (PBMCs) were isolated by Ficoll-Paque (1.077 g/l, GE healthcare, Uppsala, Sweden) gradient centrifugation. Porcine PBMCs purified by gradient centrifugation were mainly composed of lymphocytes, monocytes and a small number of macrophages [29]. For enrichment of monocytes, PBMCs were purified using the Miltenyi magnetic-activated cell sorting separation system with LS columns and antihuman CD14 antibody conjugated beads (Miltenyi Biotec GmBH, Bergissh Gladblach, Germany). The purified monocytes were cultured in RPMI-1640 supplemented with L-glutamine and 25 mM HEPES (Lonza, Walkersville, MO, USA), 100 UI/ml PenicillinG, 100 μg/ml Streptamycin (Gibco, Invitrogen), 50 μM 2-mercaptoethanol (Sigma-Aldrich, St. Louis, MO, USA) and 10% newborn calf serum (Sigma-Aldrich). For differentiation of monocytes into DCs, recombinant porcine GM-CSF (40 ng/ml) and IL-4 (40 ng/ml, R&D Systems, Minneapolis, MN, USA) were added to the culture medium and replaced every 2–3 days. Cultures were grown for 5–7 days. Lipopolysaccharides (LPS) from *Escherichia coli* 026:B6 (Sigma-Aldrich) were dosed into the DC culture from 30 ng/ml to 3 μg/ml for 18 h for DC maturation.

Immunostaining

Loosely attached DCs were scraped from the 24-well plates, centrifuged and washed with Hank's Buffered Salt Solution (HBSS). Cells were stained with a FITC-labeled mouse-antiporcine CD3 (Southern Biotech, Birmingham, AL, USA), propidium iodide (PE)-labeled mouse-antiporcine CD21 or PE- labeled human CTLA-4-mouse Ig fusion protein (Ancell,

Bayport, MN, USA) for 30 min. Samples were washed and centrifuged to remove the residual antibodies for flow cytometry. Cells were analyzed in a BD FACScan Flow Cytometer (BD Science, San Jose, CA, USA) with 10,000 cells gated on the basis of forward and side scatter and a 488-nm laser was used to excite the FITC (FL1, 530/30), PE (FL2, 585/42) and QDs (FL4, 661/16) respectively, and the data stored and processed using CellQuest Pro software (San Jose, CA, USA).

Endocytic mechanism studies

Dendritic cells were seeded in 24-well plates at 100,000 cells per well. The endocytic inhibitors nocodazole (10 μg/ml), cytochalasin D (CytD, 10 μg/ml), wortmannin (Wort, 100 ng/ml), Ly294002 (Ly, 10 μg/ml), chloroquine (CRQ, 50 μg/ml), chlorpromazine (CPM, 10 μg/ml), Y-27632 (10 μg/ml), staurosporine (SRP, 1 μg/ml), U-73122 (10 μg/ml), polyI (10 μg/ml) and fuicodan (FCD, 10 μg/ml) were purchased from Sigma-Aldrich. The concentration of the inhibitors selected was at a relative low dose based on published information and our previous studies in HEKs [15]. The doses chosen were nontoxic to DCs. Each endocytic inhibitor was predosed in the cell culture for 1 h in triplicate wells and the experiments were repeated and then dosed with QD655-COOH with or without inhibitors for another 30 min. This time frame was chosen because QD cellular uptake is at its highest based on previous research. In addition, the inhibitor has to be taken up by the cell first before it can exert an inhibitory effect. Cells were gently scraped, centrifuged, washed and resuspended in HBSS and analyzed in BD FACScanTM Flow Cytometer (BD Science) with 10,000 cells gated on the basis of forward and side scatter. A 488 nm laser was used to excite the QDs and the data stored and processed using CellQuest Pro software. The gated line separates the DCs with high fluorescent intensities from the cells in the negative control that were not treated with QDs. The inhibitory effects were calculated by comparing the fluorescence mean for each inhibitor to the control.

Fluorescence microscopy imaging

Fluorescence images were captured in the QD655-COOH channel on an Olympus X71 fluorescence microscope (Olympus, Tokyo, Japan) with Image Pro Plus software (Media Cybernetics Inc., Bethesda, MD, USA). The microscope was also equipped with a differential interference contrast (DIC) system.

Transmission electron microscopy

To observe QD655-COOH localization in cells, DCs were treated with 0.05 nM of QD655-COOH for 30 min, rinsed, fixed in Trump's fixative, routinely processed for TEM and viewed on a Philips EM208S transmission electron microscope.

Viability assays

Dendritic cells were harvested from culture dishes and seeded in 96-well plates at the density of 20,000 cells/well at 37°C in a humidified 5% CO_2 environment. The cells were exposed to RPMI-1640 medium containing 0, 0.4, 2 or 10 nM of QD655-COOH for 24 h (n = 6) and then subjected to the following viability assays. Three different viability assays were assessed for DC viability because it has been reported that some NPs may interfere with the assay itself, thereby providing inaccurate results [30]. All the viability assays were purchased from Promega (Madison, WI, USA). The absorbance, fluorescence or luminescent values were normalized by the controls and expressed as percent viability.

CellTiter 96® AQueous One Solution Cell Proliferation Assay (96AQ)

The 96AQ solution (20 μl; Promega) was added to each well (100 μl), incubated for 3 h and the absorbance at 450 nm was quantified with a Multiskan microplate spectrophotometer (Thermo LabSystems, Milford, MA, USA).

Cell Counting Kit-8

Each well (100 μl) was added with 10 μl of Cell Counting Kit-8 (Dojindo, Rockville, MD, USA), incubated for 3 h and the absorbance at 450 nm quantified with a Multiskan microplate spectrophotometer.

Alamar-Blue® assay

Culture medium was removed from each well in a 96-well black plate. The Alamar-Blue® assay solution (10μl; Invitrogen) was added to each well and cells incubated for 3 h. The fluorescence was quantitated on a Spectra Max Gemini EM spectrophotometer with an excitation wavelength of 570 nm and an emission wavelength of 585 nm ($570_{Ex}/585_{Em}$).

Other toxicity assays: ApoTox viability assay

The live-cell protease activity was measured using a fluorogenic peptide substrate (glycylphenylalanyl-aminofluorocoumarin; GF-AFC; Promega). The GF-AFC (10 ml) was transferred into 2 ml of assay buffer. Viability reagent (20 μl) containing GF-AFC substrate was added to each well, mixed by shaking and incubated for 30 min at 37°C. The fluorescence was measured on a Spectra Max Gemini EM spectrophotometer at $400_{Ex}/505_{Em}$.

GSH-GloTM glutathione assay

The medium was removed from the wells and 100 μl of The GSH-Glo™ reagent (Promega) was added to each well and incubated for 30 min followed by the addition of 100 μl luciferin detection reagent for 15 min. The luminescence was measured on a Spectra Max Gemini EM spectrophotometer.

Cytokine assay for IL-6

Cytokine analysis was conducted by enzyme-linked immunosorbant assays (R&D Systems, Wiesbaden, Germany) using commercially available kits according to the manufacturers' instructions.

Statistics

Student's t tests were used to compare two individual samples and fold changes. Values with $p < 0.05$ were considered significant from controls and marked with an asterisk. The mean values for fluorescence were calculated and the significant differences ($p < 0.05$) determined using the PROC GLM Procedure (SAS 9.1 for Windows; SAS Institute, Cary, NC, USA). When significant differences were found, multiple comparisons were performed using Tukey's Studentized Range HSD test at $p < 0.05$ level of significance.

Results

QD cellular uptake in PBMCs

Porcine PBMCs were purified using gradient centrifugation. The forward-side scatter dot plot showed PBMCs contained two cell subsets, including lymphocytes and monocytes (before purification, Figure 1A). PBMCs were dosed with 0.05 nM of QD655-COOH for 30 min followed by CD3 and CD21 staining. These results showed that 70.0% of the cells

stained with CD3 were T cells (Figure 1B). However, very few $CD3^+$ cells showed QD655-COOH (Figure 1B, before purification, upper right quadrant). Similarly, 7.3% of the PBMCs labeled with CD21 (a B-cell marker) did not show QD655-COOH uptake (Figure 1C). By comparison, there were a certain number of $CD3^-$ and $CD21^-$ cells (11.8% in Figure 1B or 11.7% in Figure 1C of total) that engulfed the QD655-COOH. Monocytes from the PBMCs were labeled with antihuman CD14 antibody conjugated beads and purified with the MACS separation system. The forward-side scatter dot plot indicated the enrichment of monocytes (Figure 1A). These cells were $CD14^+$ and were dosed with 0.05 nM QD655-COOH for 30 min, which showed that 95.5–95.7% of the cells contained QD655-COOH (Figure 1B & 1C). In addition, the dot plot distribution patterns of the QD655-$COOH^+$ cells (the lower right quadrant in Figure 1B & 1C) before and after monocyte purification were very similar, except for the difference in cell density. The above results showed that monocytes were purified and did engulf QD655-COOH NPs.

Characterization of the monocyte-derived DCs

After 5–7 days of culture, most cells increased in size compared with those before differentiation (Figure 2A). The purified monocytes may be classified into two subsets according to their MHCII expression on the cell surface and can be defined as $MHCII^-$ (fluorescence intensity = 5.2, pink, Figure 2B) and $MHCII^{low}$ (fluorescence intensity = 81.1, green, Figure 2B). Both of these two subsets have similar and low CD80/CD86 expression (fluorescence intensity = 37.2, Figure 2C) that can be recognized with the human CTLA-4-mouse Ig fusion protein. $MHCII^-$ $CD80/CD86^{low}$ cells showed higher QD655-COOH uptake compared with $MHCII^{low}$ $CD80/CD86^{low}$ cells. Purified monocytes were further differentiated into DCs with the addition of GM-CSF and IL-4. Flow cytometry indicated an increase in MHCII expression (fluorescence intensity = 285.6, Figure 2B) and a strong upregulation of CD80/CD86 expression (fluorescence intensity = 650.4, Figure 2C). Figure 2 shows that DCs have a greater efficiency for QD655-COOH cellular uptake compared with monocytes. In addition, these monocyte-derived DCs had dendritic processes that engulfed QD655-COOH (Figure 3).

Carboxylic acid-coated QDs were engulfed by monocytes & DCs

Our laboratory has shown that QD NP endocytosis depends on the surface coating and charge [13]. QDs with three different surface coatings (carboxylic coated QDs (QD655-COOH, negative charge), PEG-coated (QD655-PEG, neutral charge) and PEG-amine coated (QD655-NH_2, positive charge) were investigated to elucidate the relationship between NP cellular uptake and surface coating. As shown in Figure 4, QD655-PEG and QD655-NH_2 had no QD uptake except for some nonspecific QD staining on the monocytes and DCs. By contrast, monocytes preferred to uptake QD655-COOH (Y mean = 325.3) rather than NH_2 or PEG-coated QDs. The differentiation of monocytes into DCs greatly enhanced the uptake sixfold (Y mean = 2037.0).

To study the rate of QD cellular uptake, the QD655-COOH at 0.05 and 2 nM were dosed in DC culture from 10 min to 24 h. Cells were scraped, collected and centrifuged for flow cytometry and plotted in Figure 5. At 10 min, DCs took up QD655-COOH at the low dose (0.05 nM; Y mean = ~110, half the fluorescence intensity compared with the saturation point) and became saturated by 4 h. At the high concentration of 2 nM, QD655-COOH uptake was extremely fast at 10 min (Y mean = ~1200), but was still only approximately 35% of the saturation point by 6 h. Although QD fluorescence is more stable than the other dyes, quenching can still occur when QDs are dosed in culture media [15]. After the saturation point, the fluorescence continued to decrease, probably due to the QD quenching in the cells or, potentially, exocytosis might have occurred.

Transmission electron microscopy images depicted the ultrastructural morphology of DCs, including their dendritic processes (Figure 6A). Except for the filopodia or lamellipodia, a few cytoplasmic vacuoles were present and have been considered to be normal in DCs [31]. Treatment of QD655-COOH at 0.05 nM for 30 min revealed QD655-COOH in most of the vacuoles (Figure 6B). At the higher magnification, QD655-COOH could be identified by their ellipsoid shape and size within the vacuoles.

DC cellular uptake mechanisms of QD655-COOH

There are several endocytic pathways that DCs can utilize to uptake NPs. The cellular uptake may be regulated by some general cellular components, such as lipid rafts, cytoskeletons or endosomes. In addition, NP cellular uptake by cells may occur through macropinocytosis, clathrin or caveolae-mediated endocytosis and other more specific pathways. Since QD655-COOH have more efficient cellular uptake than PEG or PEG-amine-coated QDs, QD655-COOH was used for uptake mechanism studies. Twelve endocytic inhibitors were used to study the mechanisms of QD655-COOH in DCs and the results are summarized in Figure 7A. QD655-COOH at 0.05 nM with or without preincubation of inhibitors was incubated in the DC culture for 30 min, followed by flow cytometry quantification. In addition, some of the fluorescence images were taken and organized in Figure 7C to confirm the flow cytometry data. First, to evaluate the cytoskeletal effects on QD655-COOH endocytosis, CytD was chosen to inhibit F-actin assembly and nocodazole was used to disrupt microtubules. CytD showed a more significant reduction in QD655-COOH uptake (47.6% to control) than nocodazole (76.7%), demonstrating that F-actin dominated the QD655-COOH cellular uptake in DCs. Second, nystatin the caveolae-mediated endocytic inhibitor, CPM a clathrin-mediated endocytic inhibitor and Wort or Ly macropinocytic inhibitors were also evaluated. These results showed that QD655-COOH can be engulfed by clathrin (53.8%), while caveolae have less effect (76.7%). Wort and Ly have similar inhibitory effects on QD655-COOH cellular uptake in DCs as nystatin (67.2 and 75.2%, respectively).

Endosomes may be critical organelles to regulate the cellular uptake of QDs. Therefore, we used CRQ, a reagent that inhibits endosome acidification and is a potential endocytic inhibitor [32]. However, CRQ did not have significant inhibitory effect on the QD655-COOH cellular uptake, indicating that acidification of endosomes do not play a major role in QD655-COOH endocytosis. Other potential inhibitors such as Y-27632, a specific inhibitor of Rho-associated kinase (ROCK), U-73122 an inhibitor of phospholipase C (PLC) and SRP an inhibitor of PKC were also investigated to explore if a kinase- or phospholipase-regulated pathway could be involved in QD655-COOH uptake. Our results showed that the inhibition of PLC by U-73122 can block QD655-COOH uptake (19.6% to control), which was dose dependent (Figure 7B). SRP only had a minor inhibitory effect (SRP, 89.1%) while Y-27632 did not have an inhibitory effect (99.7%).

Previous work in our laboratory had demonstrated that QD cellular uptake in neonatal HEKs was regulated by scavenger receptors (SR) [15]. Therefore, PolyI and FCD were used to determine if DCs also utilized this pathway. Both PolyI and FCD blocked QD655-COOH cellular uptake by 18.4 and 21.8%, respectively.

QD655-COOH uptake by DCs depends on DC maturation

Lipopolysaccharides induces the maturation of DCs with an increase in cell surface marker expression (CD80/CD86) and cytokine release. At the LPS concentrations of 30 ng/ml to 1 μg/ml, CD80/CD86 expression increased nearly twofold and the capacity for DCs to take up QD655-COOH (0.05 nM for 30 min) also increased (Figure 8). A slight upregulation of QD655-COOH uptake was detected at 3 μg/ml of LPS, but this may be explained by LPS

induced DC injury. Therefore, propidium iodide and 96AQ viability assays were used to determine whether LPS induced cell death or injury to the DCs. These results did not detect dead cells at 3 μg/ml LPS (data not shown). Therefore, LPS at 3 μg/ml may have triggered another endocytic pathway.

QD655-COOH cytotoxicity in DCs evaluated with optimal viability assays

Since QDs are composed of cadmium and selenium, QDs may cause cytotoxicity at specific concentrations if these metals leach out from QDs. Since HEKs normally attach firmly to the bottom of the wells, the MTT assay would be the assay of choice. However, unlike HEKs, DCs are loosely attached to the bottom of 96-well plates. Alamar Blue, 96AQ and CCK-8 are all onestep viability assays with no extra wash steps and are considered most appropriate for suspension cells or loosely attached cells. Therefore, we used these assays to evaluate the cytotoxicity of DCs by QD655-COOH. Since, our laboratory has shown that numerous types of NPs can interfere with cytotoxicity assays in some cell types [2,7,8,30]. However, it is more likely that only the nonsoluble particles, such as carbon black, carbon nanotubes or aluminum nanomaterials, have strong interference with the assay system, while soluble or well-dispersed particles, such as QD NPs, have less effect [30]. Therefore, we also evaluated if QD655-COOH can interfere with the assay results. It was shown that QDs did not interfere with all these assays (data not shown). Our results indicated that only CCK-8 detected a small decrease in viability (96.6%) at 10 nM of QD655-COOH. The minimal viability decrease detected by the above three assays suggested that these assays may not be sensitive enough to depict the toxicity of QDs. Therefore, other cytotoxicity assays were also used to assess the mechanisms of toxicity in QDs. ApoTox assay is a fluorescence assay to evaluate the live-cell protease activity. A small viability decrease (93.2%) at 10 nM was noted, indicating QD655-COOH have a slight influence on intracellular protease activities. The GSH assay is a luminescence-based assay used to assess cellular toxicity and is also an anti-oxidant that prevents cell damage caused by reactive oxygen species in DCs [33]. We noticed a decrease in GSH levels with increased concentrations of QD655-COOH, especially at the 10 nM concentration where the GSH was 84.2% compared with control (Figure 9).

DCs are a major cell source of IL-6 within lymph nodes during primary immune responses to cutaneous antigens [34]. In addition to the viability and cytotoxicity studies, preliminary studies with the proinflammatory cytokine IL-6 were also evaluated. Compared with control (8.1 pg/ml), DCs dosed with 20 nM of QD655-COOH did not show much increase in IL-6 expression (9.2 pg/ml). By comparison, LPS at 0.8 ng/ml increased IL-6 release from DCs approximately 100-fold (788.8 pg/ml) compared with control, confirming that DCs functioned in an expected manner.

We also evaluated QD655-COOH at a high concentration (10 nM) to determine if QD655-COOH interfered with LPS-induced DC maturation with respect to cell surface marker expression of CD80/CD86. DCs were stimulated with 300 ng/ml of LPS and then dosed with or without QD655-COOH. QD655-COOH at 10 nM slightly decreased the DC CD80/CD86 expression (87.9% to control). LPS exposed to DCs for 18 h induced CD80/CD86 expression twofold compared with the control. However, QD655-COOH interfered with the LPS-induced DC maturation (80% to LPS-induced CD80/CD86 expression) (Figure 10). These results showed that QD655-COOH at 10 nM not only caused slight cytotoxicity in DCs, they may also have effect on DC maturation and activation, indicating that QD655-COOH could have an inhibitory effect on the innate immune response.

Discussion

The innate immune response may be activated by injury with exposure to infectious micro-organisms. DCs in the lung or the skin (Langerhans cells) are capable of taking up and presenting antigens for lymphocyte recognition. In addition, the maturation of DCs leads to cytokine production and release for the initiation of immune defenses. Therefore, DCs become target cells for immunotherapy by introducing NPs with functional drugs into biological systems. Biomaterial pharmaceutical NP vehicles have been used to target DCs aimed for vaccinations [35]. Antigen-carrying biodegradable poly (γ-glutamic acid) or poly(lactic-co-glycolic acid) NPs can be efficiently taken up by DCs and may be a potential vaccine adjuvant for infectious disease therapy [36,37]. However, whether the uptake is dependent on the specific antigen or relies on the types of NPs is unknown. As a result, the toxicity and mechanisms of the cellular uptake of NPs into DCs need to be elucidated to understand the immune response to NPs.

Transmission electron microscopy was used to visualize QD655-COOH subcellular localization in DCs. Figure 6 indicated that QD655-COOH were taken up by DCs and were localized in cytoplasmic vacuoles within 30 min. Intracellular vacuoles in DCs were much greater than in HEKs as determined by TEM [11]. Although 2 nM of QD655-COOH are efficiently taken up by HEKs [15], 0.05 nM concentration of QDs in DC can obtain similar fluorescence intensity within 30 min based upon fluorescence microscopy. Therefore, a lower concentration (0.05 nM) was used for this study. This was expected since the primary function of DCs is to present antigens. PEG protects poly(D,L-lactic acid) (PLA) particles from uptake by monocytes [38], which indicates that the surface coatings of NPs plays a role in altering the NP uptake in cells. Here, we showed that PEG coating on QDs also prevented the cellular uptake in DCs (Figure 4). The fact that carboxylic acid-coated QDs but not PEG- or PEG-NH_2-coated QDs were readily taken up by DCs suggest that it may be due to the recognition of the carboxylic acid groups by some organelles, receptors or epitope on the DC surface.

Cellular uptake of antigens or particles by DCs is clathrin-regulated [39]. Macropinocytosis and clathrin-dependent endocytosis are both actin-dependent processes [40,41]. Here, we showed that F-actin and clathrin pit inhibition largely decreases QD655-COOH uptake in DCs, while the inhibition of microtubules and caveolae has less of an effect on QD655-COOH endocytosis. Also, these results suggest that macropinocytosis was partially involved in the uptake mechanism. As a result, these endocytic pathways may collectively but not equally regulate QD655-COOH uptake.

Previously, we investigated these cellular uptake mechanisms with these same QDs in HEKs [15]. In that case, F-actin inhibitor did not influence QD655-COOH uptake, while disruption of microtubules interfered with QD655-COOH endocytosis by 60% (compared with the control). In addition, we showed that lipid rafts, not clathrin, caveolae or macropinocytosis, was involved in QD655-COOH uptake. The fact that DCs utilizes F-actin, clathrin and macropinocytosis to take up QD655-COOH indicates a new and different endocytic mechanism is involved in QD655-COOH cellular uptake and that the mechanism of uptake is cell type dependent.

Since DCs preferred the clathrin-regulated endocytic pathways, this suggests that some specific receptors may regulate QD655-COOH cellular uptake in DCs. Therefore, some inhibitors involved in specific endocytic pathways were investigated. The Y-27632, a specific ROCK inhibitor that inhibits actin stress fiber formation [42], U-73122 the inhibitor of PLC, SRP the inhibitor of PKC and PolyI and FCD the inhibitors for SR, were stated in the hypothesis. The relationship between SR, PKC and PLC and their role in endocytosis

has been described [43]. QD655-COOH endocytosis was blocked by PLC and SR inhibitors (Figure 7A) indicating that SR may be the receptor of recognition for QD655-COOH in DCs, while PLC may regulate this specific endocytic pathway downstream.

Endocytosis is normally downregulated after treatment of DCs with maturation stimuli, which is a hallmark of DC maturation and has been well documented [31,44]. However, the conclusion was based on antigen or endocytic tracers, which have been assumed to be macropinocytic indicators. Interestingly, our results showed QD655-COOH endocytosis was upregulated with LPS-matured DCs compared with untreated DCs (Figure 8). Recent research by Platt *et al.* showed that mature DCs downregulate macropinocytosis but continue to capture antigens and then internalized via endocytic receptors [45]. These results allowed us to hypothesize that the receptor-regulated endocytosis may dominate the cellular uptake of QD655-COOH in DCs, while macropinocytosis could be shut down in matured DCs.

Previously, it has been shown that SR class B is critical for hepatitis C endocytosis in human DCs [46]. Other studies showed that the diesel exhaust particles uptake by DCs was blocked by the SR ligand maleylated-ovalbumin [47]. We found that the SR may play an important role for QD655-COOH uptake in DCs. All of these results suggest the importance of SR on NP uptake in various studies. Interestingly, Toll-like receptor 4 ligand LPS and oxidized LDL, a SR ligand, upregulated the SR expression [47,48]. Since SR is upregulated by LPS in DCs and is the primary receptor for QDs, this may explain why mature DCs can engulf more QDs than immature DCs. Kwon *et al.* reported on the targeted delivery of microparticles with mouse DCs using DEC-205 (another DC receptor) antibodies [49]. Uptake of these microparticles by mouse bone marrow-derived DCs *in vitro* was enhanced by the antibody compared with the isotype control-coated particles. DEC-205 may be another specific pathway to investigate NP cellular uptake in DCs.

Previously, Monteiro-Riviere *et al.* showed the viability differences due to NP interference with viability assays in HEKs [30]. Therefore, it is possible to evaluate a variety of viability assays and find the optimal assay for minimal interference with NPs for a specific cell type. Viability assays showed minimal cytotoxicity of QD655-COOH at the high concentration (10 nM) in DCs. CCK-8 detected a small decrease in viability (96.6%) at 10 nM, while 96AQ and alamar Blue assays did not show a decrease in viability. Therefore, these three assays are not sensitive enough to detect the toxicity of QD655-COOH in DCs. However, intracellular protease activity and GSH level decreased, indicating some other toxicity mechanism may be involved. QD655-COOH at 10 nM also interfered with the LPS-induced CD80/CD86 expression. Previous studies in our laboratory provided evidence that QD655-COOH has some toxicity in HEKs at 20 nM, but not at the 2 nM concentrations [13]. These data indicate that QDs at specific concentrations is safe for use in biomedical applications.

Conclusion & future perspective

In conclusion, monocyte-derived DCs utilized different cytoskeletons (F-actin), substance carriers (clathrin) and endocytic pathways to take up QD655-COOH, which is different from HEK cellular uptake of QDs. The uptake of NPs also depends on the differentiation state of DCs. In addition, QD655-COOH showed minor cytotoxicity in DCs at high concentration (10 nM), although other toxic events, such as protease activity and GSH expression, concurrently occurred. For suitable nanovectors of drug delivery, NP cellular uptake mechanisms need to be conducted in the cell type of interest. As we can see from these results, cellular uptake pathways are cell specific and dependent not only on the cell type but the differentiation state of the cells.

Summary

Quantum dot NPs are novel tools used in biomedical applications, but their toxicity and mechanism of cellular uptake is unknown. Monocytes from peripheral blood were purified and differentiated into DCs. Cell differentiation showed an increase in QD655-COOH (carboxylic acid coating, with emission wavelength of 655 nm) cellular uptake. Transmission electron microscopy localized QD655-COOH in the cytoplasmic vacuoles of DCs. QD655-COOH endocytosis was recognized by clathrin and scavenger receptor and regulated by F-actin and PLC. DC maturation with LPS caused an increase in QD655-COOH uptake. Four viability assays exhibited minimal toxicity in DCs, while glutathione levels showed a significant decrease with 10 nM of QD655-COOH at 24 h. QD655-COOH exposure was associated with a decrease in CD80/CD86 expression after LPS stimulation, suggesting a suppression with DC maturation. These findings shed light on the mechanism of QD655-COOH uptake in DCs and that cellular uptake pathways are dependent on cell type and cell differentiation.

Acknowledgments

The authors would like to thank Glen Almond, North Carolina State University College of Veterinary Medicine for providing the PE conjugated antiporcine CD21 antibody.

Bibliography

Papers of special note have been highlighted as:

▪▪ of considerable interest

1. Monteiro-Riviere NA, Nemanich RJ, Inman AO, et al. Multi-walled carbon nanotube interactions with human epidermal keratinocytes. Toxicol Lett. 2005; 155:377–384. [PubMed: 15649621]
2. Monteiro-Riviere NA, Inman AO. Challenges for assessing carbon nanomaterial toxicity to the skin. Carbon. 2006; 44:1070–1078.
3. Rouse JG, Yang J, Barron AR, et al. Fullerene-based amino acid nanoparticle interactions with human epidermal keratinocytes. Toxicol In vitro. 2006; 20:1313–1320. [PubMed: 16759832]
4. Zhang LW, Yang J, Barron AR, et al. Endocytic mechanisms and toxicity of a functionalized fullerene in human cells. Toxicol Lett. 2009; 191:149–157. [PubMed: 19723571]
5. Zhang LW, Zeng L, Barron AR. Biological interactions of functionalized single-wall carbon nanotubes in human epidermal keratinocytes. Int J Toxicol. 2007; 26:103–113. [PubMed: 17454250]
6. Chithrani BD, Ghazani AA, Chan WC. Determining the size and shape dependence of gold nanoparticle uptake into mammalian cells. Nano Lett. 2006; 6:662–668. [PubMed: 16608261]
7. Samberg ME, Oldenburg SJ, Monteiro-Riviere NA. Evaluation of silver nanoparticle toxicity in skin *in vivo* and keratinocytes *in vitro*. Environ Health Perspect. 2010; 118:407–413. [PubMed: 20064793]
8. Monteiro-Riviere NA, Oldenburg SJ, Inman AO. Interactions of aluminum nanoparticles with human epidermal keratinocytes. J Appl Toxicol. 2010; 30:276–285. [PubMed: 20013751]
9. Duan H, Nie S. Cell-penetrating quantum dots based on multivalent and endosome-disrupting surface coatings. J Am Chem Soc. 2007; 129:3333–3338. [PubMed: 17319667]
10. Jaiswal JK, Mattoussi H, Mauro JM, et al. Longterm multiple color imaging of live cells using quantum dot bioconjugates. Nat Biotechnol. 2003; 21:47–51. [PubMed: 12459736]
11. Zhang LW, Yu WW, Colvin VL, et al. Biological interactions of quantum dot nanoparticles in skin and in human epidermal keratinocytes. Toxicol Appl Pharmacol. 2008; 228:200–211. [PubMed: 18261754]
12. Ryman-Rasmussen JP, Riviere JE, Monteiro-Riviere NA. Penetration of intact skin by quantum dots with diverse physicochemical properties. Toxicol Sci. 2006; 91:159–65. [PubMed: 16443688]

13. Ryman-Rasmussen JP, Riviere JE, Monteiro-Riviere NA. Surface coatings determine cytotoxicity and irritation potential of quantum dot nanoparticles in epidermal keratinocytes. J Invest Dermatol. 2007; 127:143–153. [PubMed: 16902417]

14. Ryman-Rasmussen JP, Riviere JE, Monteiro-Riviere NA. Variables influencing interactions of untargeted quantum dot nanoparticles with skin cells and identification of biochemical modulators. Nano Lett. 2007; 7:1344–1348. [PubMed: 17408303]

15▪. Zhang LW, Monteiro-Riviere NA. Mechanisms of quantum dot nanoparticle cellular uptake. Toxicol Sci. 2009; 110:138–155. Describes the mechanism of nanoparticle cellular uptake. [PubMed: 19414515]

16. Sallusto F, Cella M, Danieli C, et al. Dendritic cells use macropinocytosis and the mannose receptor to concentrate macromolecules in the major histocompatibility complex class II compartment: downregulation by cytokines and bacterial products. J Exp Med. 1995; 182:389–400. [PubMed: 7629501]

17. Geissmann F, Prost C, Monnet JP, et al. Transforming growth factor β1, in the presence of granulocyte/macrophage colony-stimulating factor and interleukin 4, induces differentiation of human peripheral blood monocytes into dendritic Langerhans cells. J Exp Med. 1998; 187:961–966. [PubMed: 9500798]

18. Agger R, Petersen MS, Toldbod HE, et al. Characterization of murine dendritic cells derived from adherent blood mononuclear cells *in vitro*. Scand J Immunol. 2000; 52:138–147. [PubMed: 10931381]

19. Howard CJ, Brooke GP, Werling D, et al. Dendritic cells in cattle: phenotype and function. Vet Immunol Immunopathol. 1999; 72:119–124. [PubMed: 10614501]

20. Cambi A, Lidke DS, Arndt-Jovin DJ, et al. Ligand-conjugated quantum dots monitor antigen uptake and processing by dendritic cells. Nano Lett. 2007; 7:970–977. [PubMed: 17388641]

21. Elamanchili P, Diwan M, Cao M, et al. Characterization of poly (D,L-lactic-co-glycolic acid) based nanoparticulate system for enhanced delivery of antigens to dendritic cells. Vaccine. 2004; 22:2406–2412. [PubMed: 15193402]

22. Manolova V, Flace A, Bauer M, et al. Nanoparticles target distinct dendritic cell populations according to their size. Eur J Immunol. 2008; 38:1404–1413. [PubMed: 18389478]

23. Coester C, Nayyar P, Samuel J. *In vitro* uptake of gelatin nanoparticles by murine dendritic cells and their intracellular localisation. Eur J Pharm Biopharm. 2006; 62:306–314. [PubMed: 16316749]

24. Nabiev I, Mitchell S, Davies A, et al. Nonfunctionalized nanocrystals can exploit a cell's active transport machinery delivering them to specific nuclear and cytoplasmic compartments. Nano Lett. 2007; 7:3452–3461. [PubMed: 17949046]

25. Hochrein H, Wagner H. Of men, mice and pigs: looking at their plasmacytoid dendritic cells. Immunology. 2004; 112:26–27. [PubMed: 15096180]

26. Carrasco CP, Rigden RC, Schaffner R, et al. Porcine dendritic cells generated *in vitro*: morphological, phenotypic and functional properties. Immunology. 2001; 104:175–184. [PubMed: 11683958]

27. Raymond CR, Wilkie BN. Toll-like receptor, MHC II, B7 and cytokine expression by porcine monocytes and monocytederived dendritic cells in response to microbial pathogenassociated molecular patterns. Vet Immunol Immunopathol. 2005; 107:235–247. [PubMed: 15998543]

28. Summerfield A, McCullough KC. The porcine dendritic cell family. Dev Comp Immunol. 2009; 33:299–309. [PubMed: 18582937]

29. van Furth R, Cohn ZA, Hirsch JG, et al. The mononuclear phagocyte system: a new classification of macrophages, monocytes, and their precursor cells. Bull World Health Organ. 1972; 46:845–852. [PubMed: 4538544]

30. Monteiro-Riviere NA, Inman AO, Zhang LW. Limitations and relative utility of screening assays to assess engineered nanoparticle toxicity in a human cell line. Toxicol Appl Pharmacol. 2009; 234:222–235. [PubMed: 18983864]

31. Paillot R, Laval F, Audonnet JC, et al. Functional and phenotypic characterization of distinct porcine dendritic cells derived from peripheral blood monocytes. Immunology. 2001; 102:396–404. [PubMed: 11328373]

32. van Weert AW, Dunn KW, Gueze HJ, et al. Transport from late endosomes to lysosomes, but not sorting of integral membrane proteins in endosomes, depends on the vacuolar proton pump. J Cell Biol. 1995; 130:21–24.
33. Yamada H, Arai T, Endo N, et al. LPS-induced ROS generation and changes in glutathione level and their relation to the maturation of human monocyte-derived dendritic cells. Life Sci. 2005; 78:926–933. [PubMed: 16280135]
34. Hope JC, Cumberbatch M, Fielding I. Identification of dendritic cells as a major source of interleukin-6 in draining lymph nodes following skin sensitization of mice. Immunology. 1995; 86:441–447. [PubMed: 8550083]
35. Reddy ST, Swartz MA, Hubbell JA. Targeting dendritic cells with biomaterials: developing the next generation of vaccines. Trends Immunol. 2006; 27:573–579. [PubMed: 17049307]
36. Cruz LJ, Tacken PJ, Fokkink R, et al. Targeted PLGA nano-but not microparticles specifically deliver antigen to human dendritic cells via DC-SIGN *in vitro*. J Control Release. 2010; 144:118–126. [PubMed: 20156497]
37. Uto T, Wang X, Sato K, et al. Targeting of antigen to dendritic cells with poly(γ-glutamic acid) nanoparticles induces antigen-specific humoral and cellular immunity. J Immunol. 2007; 178:2979–2986. [PubMed: 17312143]
38. Leroux JC, De Jaeghere F, Anner B, et al. An investigation on the role of plasma and serum opsonins on the internalization of biodegradable poly(D,L-lactic acid) nanoparticles by human monocytes. Life Sci. 1995; 57:695–703. [PubMed: 7637541]
39. Garrett WS, Chen LM, Kroschewski R, et al. Developmental control of endocytosis in dendritic cells by Cdc42. Cell. 2000; 102:325–34. [PubMed: 10975523]
40. Merrifield CJ, Feldman ME, Wan L, et al. Imaging actin and dynamin recruitment during invagination of single clathrin-coated pits. Nat Cell Biol. 2002; 4:691–698. [PubMed: 12198492]
41. Kruth HS, Jones NL, Huang W, et al. Macropinocytosis is the endocytic pathway that mediates macrophage foam cell formation with native low density lipoprotein. J Biol Chem. 2005; 280:2352–2360. [PubMed: 15533943]
42. Katoh K, Kano Y, Amano M, et al. Rho-kinase-mediated contraction of isolated stress fibers. J Cell Biol. 2001; 153:569–584. [PubMed: 11331307]
43. Makranz C, Cohen G, Baron A, et al. Phosphatidylinositol 3-kinase, phosphoinositide-specific phospholipase-Cγ and protein kinase-C signal myelin phagocytosis mediated by complement receptor-3 alone and combined with scavenger receptor-AI/II in macrophages. Neurobiol Dis. 2004; 15:279–286. [PubMed: 15006698]
44. Sallusto F, Lanzavecchia A. Efficient presentation of soluble antigen by cultured human dendritic cells is maintained by granulocyte/macrophage colony-stimulating factor plus interleukin 4 and downregulated by tumor necrosis factor α. J Exp Med. 1994; 179:1109–1118. [PubMed: 8145033]
45. Platt CD, Ma JK, Chalouni C. Mature dendritic cells use endocytic receptors to capture and present antigens. Proc Natl Acad Sci USA. 2010; 107:4287–4292. [PubMed: 20142498]
46. Barth H, Schnober EK, Neumann-Haefelin C, et al. Scavenger receptor class B is required for hepatitis C virus uptake and cross-presentation by human dendritic cells. J Virol. 2008; 82:3466–3479. [PubMed: 18216094]
47. Taront S, Dieudonn A, Blanchard S, et al. Implication of scavenger receptors in the interactions between diesel exhaust particles and immature or mature dendritic cells. Part Fibre Toxicol. 2009; 13:6–9.
48. Nickel T, Schmauss D, Hanssen H, et al. oxLDL uptake by dendritic cells induces upregulation of scavenger-receptors, maturation and differentiation. Atherosclerosis. 2009; 205:442–450. [PubMed: 19203752]
49. Kwon YJ, James E, Shastri N, et al. *In vivo* targeting of dendritic cells for activation of cellular immunity using vaccine carriers based on pH-responsive microparticles. Proc Natl Acad Sci USA. 2005; 102:18264–18268. [PubMed: 16344458]

Executive summary

- Monocytes from the peripheral blood were purified and differentiated into dendritic cells (DCs). The cell differentiation increased the cellular uptake of carboxylic acid coated quantum dots (QD655-COOH, carboxylic acid coating and emission wavelength at 655 nm).
- Transmission electron microscopy localized QD655-COOH in the cytoplasmic vacuoles of DCs.
- QD655-COOH endocytosis was recognized by clathrin and scavenger receptor and regulated by F-actin and phospholipase C.
- DC maturation with lipopolysaccharide caused an increase in QD655-COOH uptake.
- Viability assays exhibited minimal toxicity in DCs, while glutathione levels showed a significant decrease with 10 nM of QD655-COOH at 24 h.
- QD655-COOH exposure was associated with a decrease in CD80/CD86 expression after lipopolysaccharide stimulation, suggesting a suppression with DC maturation.

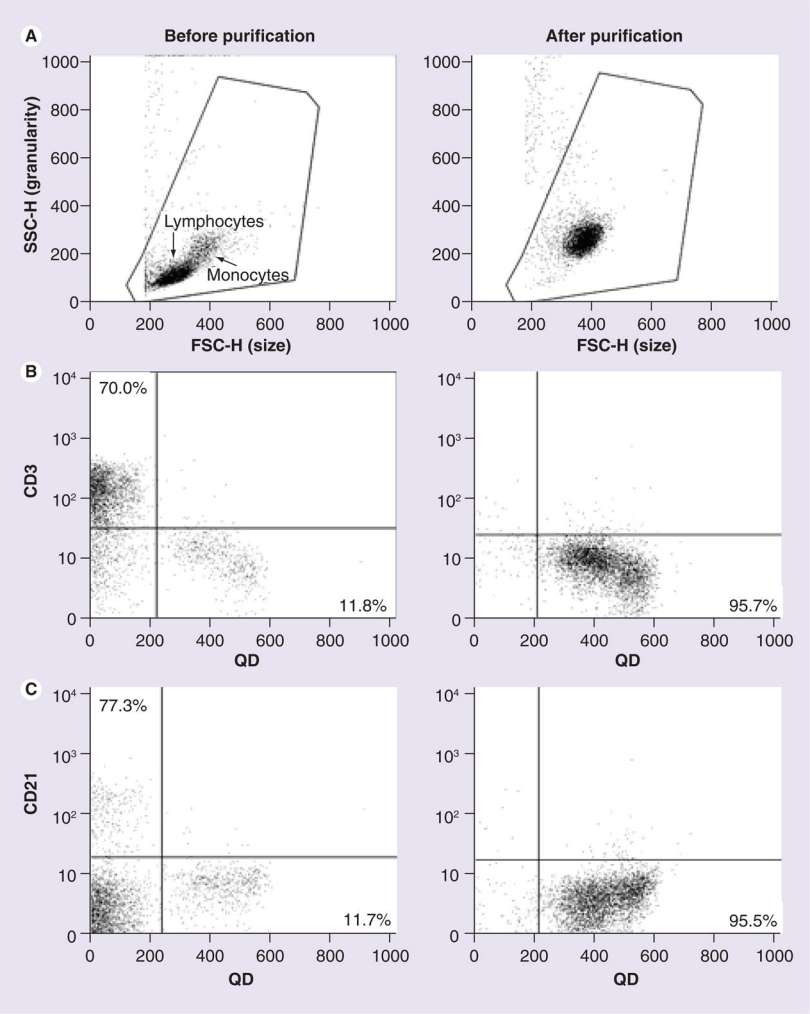

Figure 1. Peripheral blood mononuclear cell and monocyte characterization and QD655-COOH uptake (flow cytometry)

Peripheral blood mononuclear cells (PBMCs) were isolated by Ficoll-Paque gradient centrifugation and monocytes were purified using the MACS separation system with CD14 antibody conjugated beads. Left column, dot plot for PBMCs (before purification); right column, dot plot for monocytes (after purification). **(A)** The forward-side scatter dot plots depicting lymphocytes and monocytes. **(B & C)** QD655-COOH at 0.05 nM were incubated with PBMCs or monocytes for 30 min. Cells were labeled with CD3 (T cell marker **[B]**) and CD21 (B-cell marker **[C]**). The plots shown are representative of three independent experiments with similar results.

FSC-H: Forward scatter height; QD: Quantum dot; SSC-H: Side scatter height.

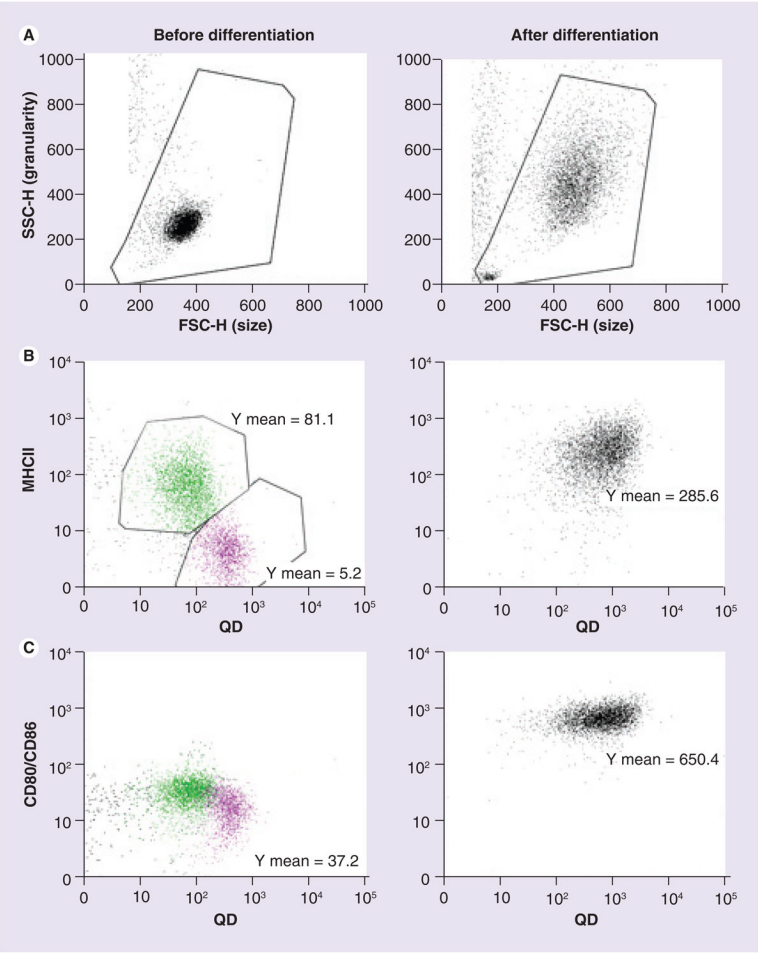

Figure 2. Surface marker expression of monocytes and dendritic cells

Monocytes were differentiated into dendritic cells (DCs) with GM-CSF and IL-4. Left column, dot plot for monocytes (before differentiation); right column, dot plot for monocyte-derived DCs (after differentiation). **(A)** The forward-side scatter dot plots depict monocytes or DCs. **(B & C)** QD655-COOH at 0.05 nM were incubated with monocytes or DC culture for 30 min. Monocytes and DCs were stained with MHCII **(B)** and CD80/CD86 **(C)**. Green and pink dots indicate the two different cell subsets, respectively. Plots shown are representative of three independent experiments with similar results.

FSC-H: Forward scatter height; QD: Quantum dot; SSC-H: Side scatter height.

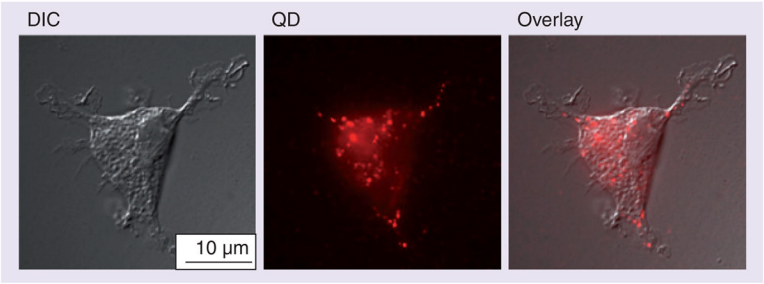

Figure 3. QD655-COOH cellular uptake in dendritic cells imaged by fluorescence microscopy
QD655-COOH at 0.05 nM were incubated with dendritic cells for 30 min. Fluorescence images were captured in the DIC mode and QD channel.
DIC: Differential interference contrast; QD: Quantum dot.

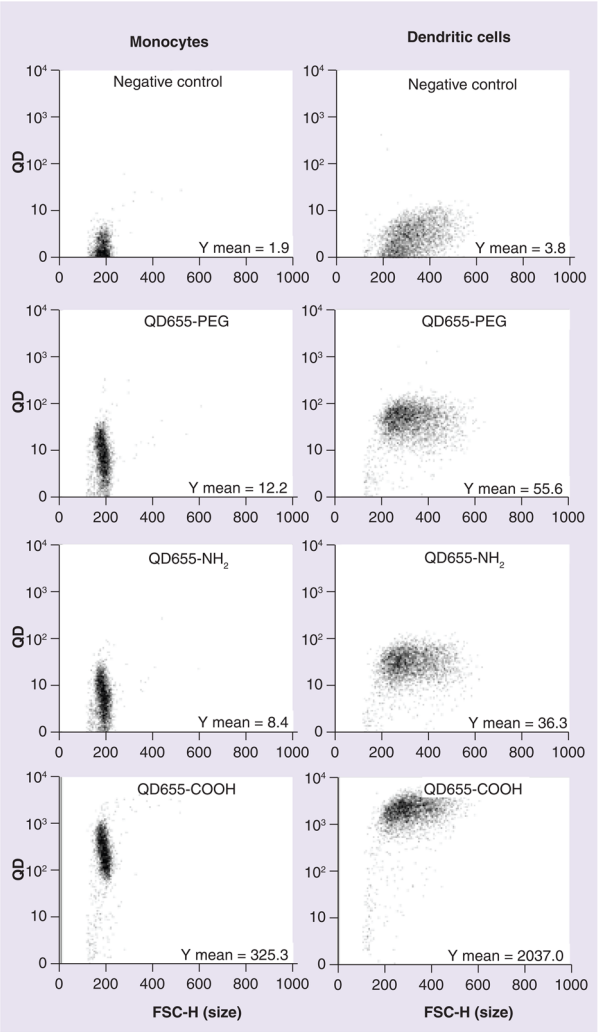

Figure 4. Quantum dot cellular uptake in monocytes and dendritic cells depends on the surface coating of quantum dots

QD655-PEG, QD655-NH_2 and QD655-COOH at 2 nM were dosed in monocytes or dendritic cells for 30 min followed by flow cytometry for QD fluorescence intensity. The plots shown are representative of three independent experiments with similar results.
FSC-H: Forward scatter height; PEG: Polyethylene glycol; QD: Quantum dot.

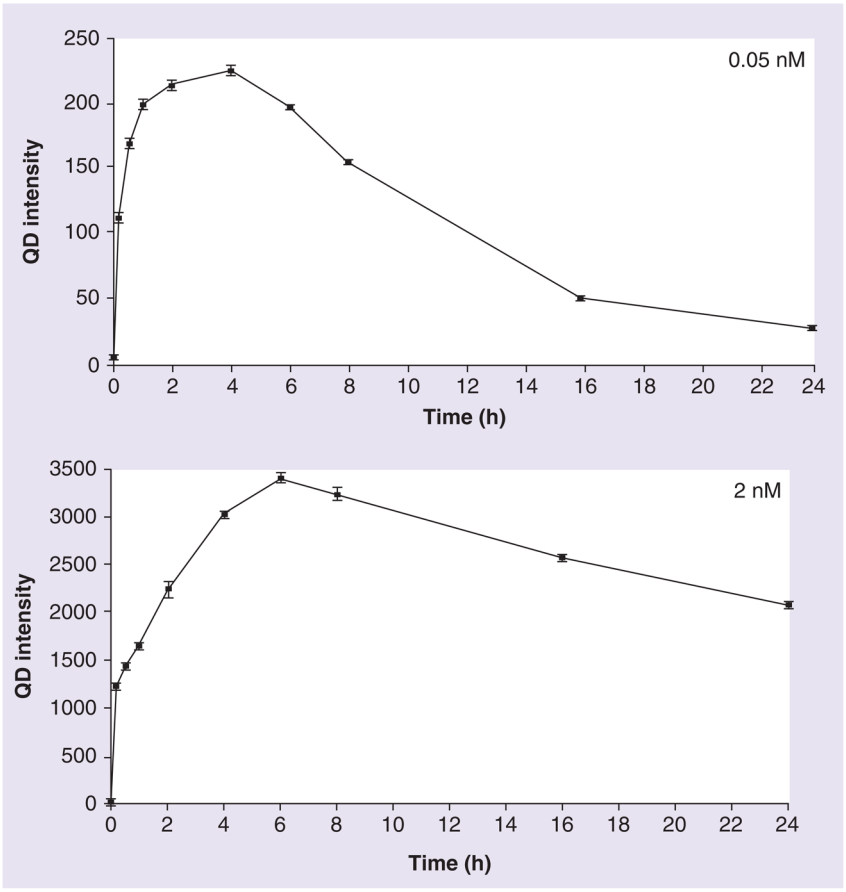

Figure 5. QD655-COOH cellular uptake vs time

QD655-COOH of 0.05 or 2 nM were incubated in dendritic cells for 10 min, 30 min, 1 h, 2 h, 4 h, 6 h, 8 h, 16 h and 24 h (n = 3/treatment). The mean QD fluorescence intensity in cells were evaluated by flow cytometry at each time point.

QD: Quantum dot.

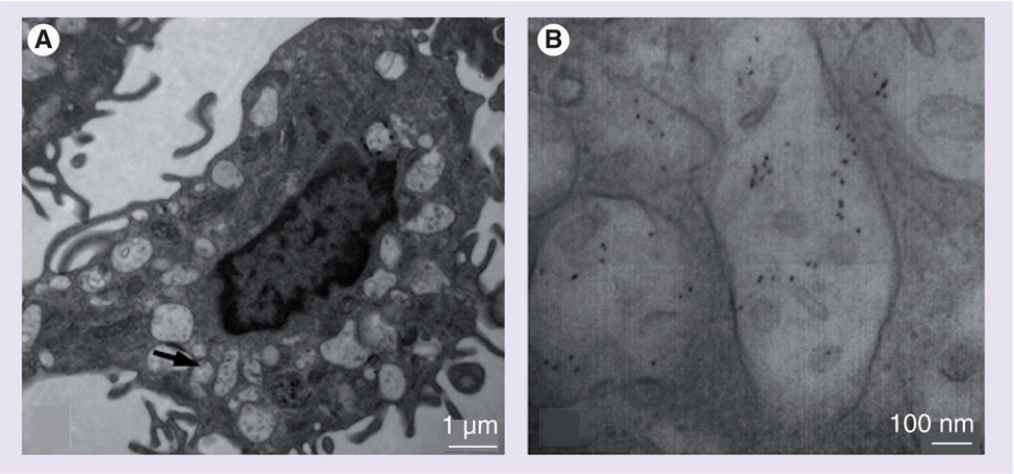

Figure 6. Transmission electron micrograph of QD655-COOH in dendritic cells

QD655-COOH of 0.05 nM were incubated in dendritic cells for 30 min. **(A)** Transmission electron micrograph images showed dendritic cells with cytoplasmic vacuoles. **(B)** Higher magnification for the arrows indicated in **(A)**, showing QD655-COOH in the vacuoles.

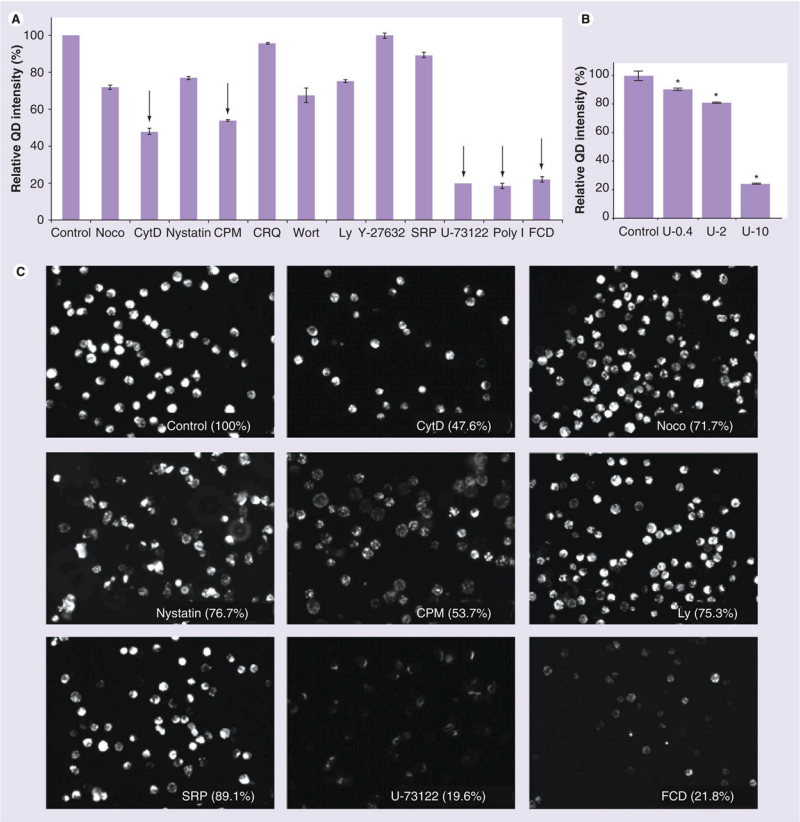

Figure 7. QD655-COOH cellular uptake mechanisms in dendritic cells

(A) Mocodazole (10 μg/ml), CytD (10 μg/ml), Wort (100 ng/ml), Ly (10 μg/ml), CRQ (50 μg/ml), CPM (10 μg/ml), Y-27632 (10 μg/ml), SRP (1 μg/ml), U-73122 (10 μg/ml), polyI (10 μg/ml) and FCD (10 μg/ml) were used to investigate the QD655-COOH uptake inhibition at indicated concentration described in the 'Materials and methods' section. QD655-COOH at 0.05 nM were incubated with dendritic cells (DCs) associated or without each inhibitor preincubation. The mean QD fluorescence intensity in the cells was evaluated by flow cytometry and normalized to the control (without inhibitors; n = 3/treatment). The intensities for inhibitor treated samples were all statistically lower ($p \leq 0.05$) than the control (100%) except for Y-27632. The inhibitors with endocytic inhibitory effects ≥ approximately 50% are indicated by arrows. **(B)** QD655-COOH uptake inhibition by U-73122 is concentration dependent. QD655-COOH at 0.05 nM were incubated with DCs associated with or without U-73122 at 0.4, 2 and 10 μg/ml. DCs were collected and evaluated by flow cytometry for QD655-COOH fluorescence intensity and normalized to the control (n = 3/treatment). *$p < 0.05$ indicates significant differences between the U-73122 dosed group and control. **(C)** QD655-COOH inhibitory effects by some of the endocytic inhibitors (CytD, Noco, Nystatin, CPM, Ly, SRP, U-73122 and FCD) imaged by fluorescence microscopy. The image for each inhibitor was marked with the percentage fluorescence intensity compared with control. Each cell is 8–10 μm in diameter.
CPM: Chlorpromazine; CRQ: Chloroquine; CytD: Cytochalasin D; FCD: Fuicodan; Ly: Ly294002; QD: Quantum dot; SRP: Staurosporine; Wort: Wortmannin.

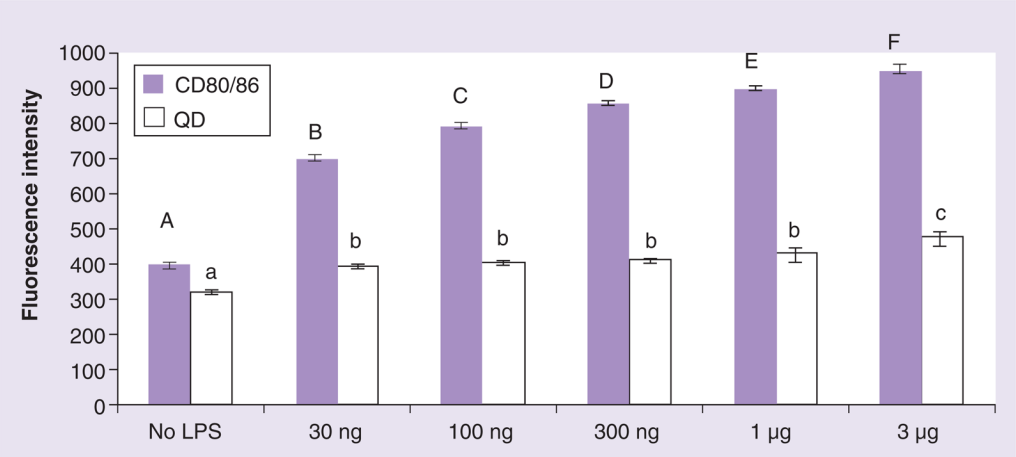

Figure 8. Dendritic cell maturation and QD655-COOH uptake

Dendritic cells (DCs) were stimulated by LPS from 30 ng/ml to 3 µg/ml for 18 h, followed by 0.05 nM of QD655-COOH incubation with DC culture for 30 min (n = 3/treatment). DCs were stained with CD80/CD86 and the cells were collected and evaluated by flow cytometry for QD fluorescence intensity. CD80/CD86 fluorescence with different letters **(A–F)** and QD fluorescence **(a–c)** staining histogram denote mean values that are statistically different at $p < 0.05$. Data are expressed as mean ± SEM.

LPS: Lipopolysaccharide; QD: Quantum dot.

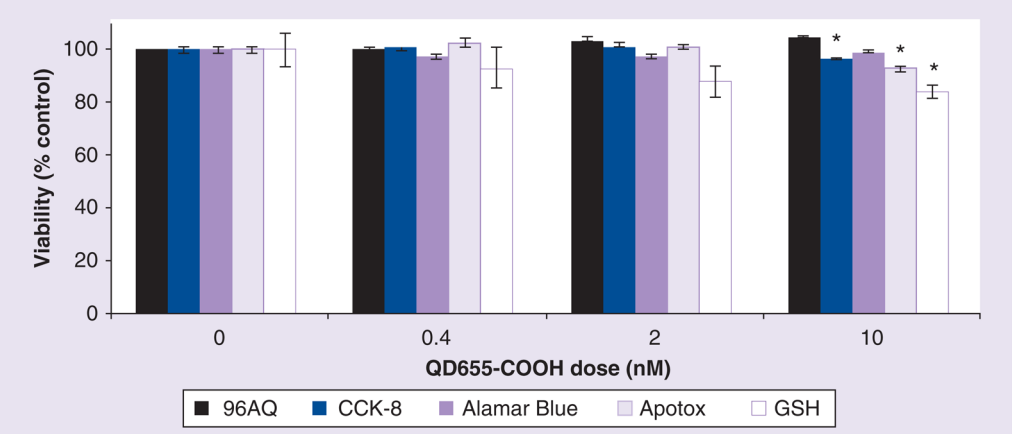

Figure 9. Viability of dendritic cells dosed with QD655-COOH

96AQ, CCK-8, Alamar Blue, ApoTox and GSH assays were performed for cytotoxicity. QD655-COOH at 0, 0.4, 2 and 10 nM were dosed in the dendritic cell culture in 96-well plates for 24 h (n = 6/treatment). Data are expressed as mean ± SEM. *$p \leq 0.05$ indicates significant differences between the dosed group and control within each assay.

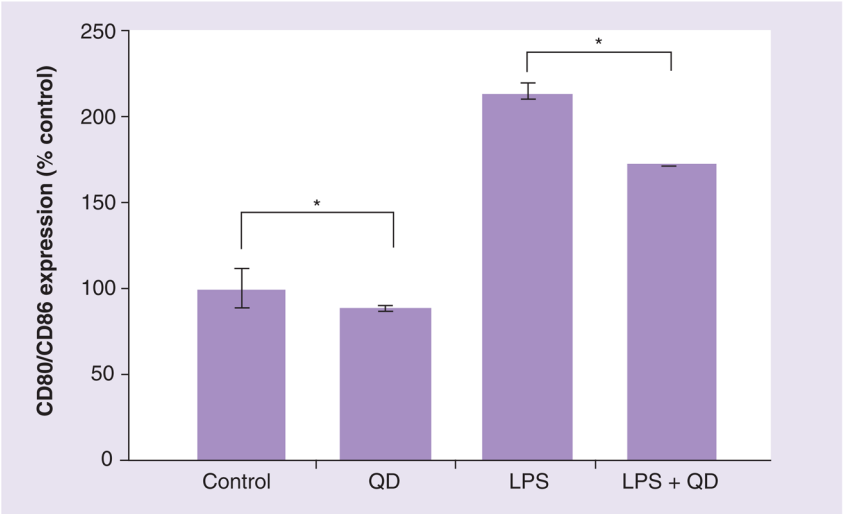

Figure 10. QD655-COOH effects on dendritic cell surface marker expression

LPS at 300 ng/ml were used for maturation of dendritic cells (DCs). QD655-COOH at 10 nM were incubated with immature and mature DCs for 24 h (n = 3/treatment). DCs were stained with CD80/CD86 and quantified by flow cytometry. *$p < 0.05$ indicates significant differences between the basal control (or LPS treated control) and corresponding QD dosed sample.

LPS: Lipopolysaccharide; QD: Quantum dot.